frontiers | Frontiers in Marine Science

TYPE Original Research
PUBLISHED 27 October 2023
DOI 10.3389/fmars.2023.1249115

OPEN ACCESS

EDITED BY
Margarita Fernández Tejedor,
Institute of Agrifood Research and Technology (IRTA), Spain

REVIEWED BY
Dengzhou Gao,
East China Normal University, China
Annie Bourbonnais,
University of South Carolina, United States

*CORRESPONDENCE
Heather J. Forrer
hforrer@fsu.edu

RECEIVED 28 June 2023
ACCEPTED 12 October 2023
PUBLISHED 27 October 2023

CITATION
Forrer HJ, Bonnet S, Thomas RK, Grosso O, Guieu C and Knapp AN (2023) Quantifying N_2 fixation and its contribution to export production near the Tonga-Kermadec Arc using nitrogen isotope budgets. *Front. Mar. Sci.* 10:1249115. doi: 10.3389/fmars.2023.1249115

Quantifying N_2 fixation and its contribution to export production near the Tonga-Kermadec Arc using nitrogen isotope budgets

Heather J. Forrer[1]*, Sophie Bonnet[2], Rachel K. Thomas[1], Olivier Grosso[2], Cecile Guieu[3] and Angela N. Knapp[1]

[1]Earth, Ocean, and Atmospheric Science Department, Florida State University, Tallahassee, FL, United States, [2]Aix Marseille University, Université de Toulon, CNRS, IRD, MIO Marseille, France, [3]Laboratoire d'Oceanographie de Villefranche, CNRS, Sorbonne University, Villefranche-sur-mer, France

The spatial distribution of marine di-nitrogen (N_2) fixation informs our understanding of the sensitivities of this process as well as the potential for this new nitrogen (N) source to drive export production, influencing the global carbon (C) cycle and climate. Using geochemically-derived $\delta^{15}N$ budgets, we quantified rates of N_2 fixation and its importance for supporting export production at stations sampled near the southwest Pacific Tonga-Kermadec Arc. Recent observations indicate that shallow (<300 m) hydrothermal vents located along the arc provide significant dissolved iron to the euphotic zone, stimulating N_2 fixation. Here we compare measurements of water column $\delta^{15}N_{NO3+NO2}$ with sinking particulate $\delta^{15}N$ collected by short-term sediment traps deployed at 170 m and 270 m at stations in close proximity to subsurface hydrothermal activity, and the $\delta^{15}N$ of N_2 fixation. Results from the $\delta^{15}N$ budgets yield high geochemically-based N_2 fixation rates (282 to 638 μmol N m^{-2} d^{-1}) at stations impacted by hydrothermal activity, supporting 64 to 92% of export production in late spring. These results are consistent with contemporaneous $^{15}N_2$ uptake rate estimates and molecular work describing high *Trichodesmium* spp. and other diazotroph abundances associated with elevated N_2 fixation rates. Further, the $\delta^{15}N$ of sinking particulate N collected at 1000 m over an annual cycle revealed sinking fluxes peaked in the summer and coincided with the lowest $\delta^{15}N$, while lower winter sinking fluxes had the highest $\delta^{15}N$, indicating isotopically distinct N sources supporting export seasonally, and aligning with observations from most other $\delta^{15}N$ budgets in oligotrophic regions. Consequently, the significant regional N_2 fixation input to the late spring/summer Western Tropical South Pacific results in the accumulation of low-$\delta^{15}N_{NO3+NO2}$ in the upper thermocline that works to lower the elevated $\delta^{15}N_{NO3+NO2}$ generated in the oxygen deficient zones in the Eastern Tropical South Pacific.

KEYWORDS

N_2 fixation, nitrate d15N, Tonga Arc, South Pacific, hydrothermal vents, d15N budget

1 Introduction

The biological fixation of dinitrogen (N_2) gas, mediated primarily by marine prokaryotes ("diazotrophs"), is the largest source of newly fixed nitrogen (N) to the global ocean (Gruber, 2004; Landolfi et al., 2018), fertilizing primary productivity and supporting carbon (C) export (Dugdale and Goering, 1967; Karl et al., 1997; Capone, 2001; Capone et al., 2005). The global rate and distribution of marine N_2 fixation remains uncertain, although geochemical and biological observations indicate significant N_2 fixation rates occur in both the Tropical Atlantic (Gruber, 2004; Capone et al., 2005; Mahaffey, 2005; Marconi et al., 2017) as well as the Western Tropical South Pacific (WTSP) (Berthelot et al., 2017; Bonnet et al., 2017; Caffin et al., 2018; Knapp et al., 2018). These high rates of N_2 fixation in the Tropical Atlantic are consistent with locations of elevated rates of atmospheric dust deposition (Jickells et al., 2005; Mahowald et al., 2005; Conway and John, 2014; Xu and Weber, 2021), while emerging evidence in the WTSP describes the significance of hydrothermally sourced iron (Fe) (Guieu et al., 2018; Bonnet et al., 2023b) meet the high Fe requirements of diazotrophs (Berman-Frank et al., 2001; Kustka et al., 2003) in the region. Indeed, Fe and phosphorus availability are thought to primarily influence the spatial distribution of marine N_2 fixation (Moore et al., 2009; Monteiro et al., 2011; Dutkiewicz et al., 2012; Weber and Deutsch, 2014).

A long-standing goal of marine N_2 fixation research is to better characterize the marine diazotroph community and their sensitivity to environmental fluctuations, while relating these to their regional distributions and consequential N_2 fixation fluxes (Mahaffey, 2005; Moisander et al., 2010; Sohm et al., 2011). Diazotrophs are identified by the nitrogenase (*nifH*) gene that encodes for the Fe binding protein of the *nifH* operon (Zehr et al., 1998; Zehr and Turner, 2001; Turk-Kubo et al., 2012). Common marine proteobacterial (e.g., alpha-, beta- gamma-, delta-) and cyanobacterial diazotroph types include: 1) non-heterocystous filamentous (e.g., *Trichodesmium* spp.), 2) heterocystous filamentous (e.g., *Richelia*), and 3) unicellular (e.g., *Crocosphaera* spp.) (Capone et al., 1997; Luo et al., 2012; Moisander et al., 2014). Historically, high rates of N_2 fixation by these and other diazotrophs have been associated with warm (>25 °C), nitrate (NO_3^-)- and ammonium (NH_4^+)-depleted, Fe-rich surface waters (Kustka et al., 2003; Staal et al., 2003; Bonnet et al., 2009). The impact Fe has on the intra-basin distribution of N_2 fixation rates is particularly evident in the South Pacific, with low Fe supply associated with low rates of N_2 fixation in the Eastern Tropical South Pacific (ETSP) (Dekaezemacker et al., 2013; Knapp et al., 2016a). While historically atmospheric deposition has been considered the primary source of Fe fueling marine diazotrophy, the WTSP surface waters appear relatively unique, with the primary Fe supply thought to originate from shallow (≤300 m) hydrothermal vents, particularly in the Lau Basin (Guieu et al., 2018; Tilliette et al., 2022; Bonnet et al., 2023b).

Biological tools have been used to calculate short-term N_2 fixation rates (e.g., Montoya et al., 2004; Capone et al., 2005; Mulholland et al., 2019) and identify marine diazotrophic potential (Turk-Kubo et al., 2012; Stenegren et al., 2018; Meiler et al., 2022). However, the contribution of N_2 fixation to export production is primarily estimated using a geochemically-derived "$\delta^{15}N$" budget over short timescales (Casciotti et al., 2008; Bourbonnais et al., 2009; White et al., 2013) as well as annual cycles (Böttjer et al., 2017). The "$\delta^{15}N$" budget uses a two end-member mixing model to compare the isotopic composition ($\delta^{15}N$) of exported particulate organic matter captured in a sediment trap (PN_{sink}) to the $\delta^{15}N$ of N_2 fixation inputs (-1‰) (Hoering and Ford, 1960; Minagawa and Wada, 1986; Carpenter et al., 1997) and subsurface NO_3^- (measured at each location, where $\delta^{15}N$ (‰ vs. air) = $[(({}^{15}N/{}^{14}N)_{sample}/({}^{15}N/{}^{14}N)_{AIR})-1]x1000$) (Altabet, 1988; Karl et al., 1997; Dore et al., 2002; Casciotti et al., 2008; Bourbonnais et al., 2009; White et al., 2013). Most prior $\delta^{15}N$ budgets indicate that N_2 fixation supports <20% of export production in oligotrophic regions. In the North Pacific and ETSP, ≤25% of export production is estimated to be supported by N_2 fixation (Casciotti et al., 2008; Knapp et al., 2016a; Böttjer et al., 2017), although that 25% is likely not equally distributed over an annual cycle. Specifically, summertime stratification is believed to promote N_2 fixation-supported export, while the deepening of the wintertime mixed layer promotes NO_3^-supported export production (Casciotti et al., 2008; Böttjer et al., 2017). In contrast to other $\delta^{15}N$ budgets from oligotrophic regions, a recent study from the WTSP describes particularly large contributions of N_2 fixation to export production (>50%) during the late summer and early autumn (Knapp et al., 2018). However, it remains unclear whether N_2 fixation supports a meaningful fraction of N export in the WTSP annually. Here we apply a $\delta^{15}N$ budget to samples collected in shallow (170 m and 270 m), short-term drifting sediment traps to evaluate the importance of N_2 fixation-supported export production during the late spring. Additionally, we use sinking material collected over the course of a year in a deep (1000 m), moored sediment trap to evaluate seasonal trends in the $\delta^{15}N$ of exported particulate organic matter relative to the $\delta^{15}N$ for sources of new N to surface waters. We compare the geochemically-derived N_2 fixation rates from the short-term $\delta^{15}N$ budgets with $^{15}N_2$ incubation-based rates and estimates of diazotroph abundance, and evaluate these results in the context of previous regional and global N_2 fixation rate estimates, as well as seasonal trends extracted from the deep, moored trap.

2 Methods

2.1 Sample collection

Sample collection was conducted as part of the GEOTRACES TONGA (shallow hydroThermal sOurces of trace elemeNts: potential impacts on biological productivity and the bioloGicAl carbon pump) research cruises (doi.org/10.17600/18000884) aboard the *R/V L'Atalante* in November 2019 and *R/V Alis* in

October 2020, with both cruises leaving from and returning to Nouméa, New Caledonia. The 2019 primary cruise collected samples at 13 stations along a roughly zonal transect at ~20° S, sampling Melanesian waters (MW), the Lau Basin (LB), and crossing the Tonga-Kermadec Arc into the deeper South Pacific Gyre (SPG). In 2020, samples were collected at four stations in MW and the LB (Figure 1). On both cruises, water column samples (n=200) for nitrate + nitrite ($[NO_3^-+NO_2^-]$) concentration and $\delta^{15}N$ analysis were collected from Niskin or GoFlo bottles deployed on conductivity, temperature, and depth (CTD), TOW (small, classical CTD with 12 Niskin bottles), or trace metal clean (TMC) rosettes equipped with sensors. At discrete depths from each of the casts, 60 mL of 0.2 µm filtered seawater were collected in duplicate and stored in acid and deionized water-washed, sample-rinsed (three times) high-density polyethylene bottles. These samples were then immediately frozen at -20° C and subsequently sent to Florida State University for post cruise analysis.

Short-term Particle Interceptor Traps [PIT, collecting area of 0.0085 m^2, aspect ratio of 6.7, and filled with 0.2 µm filtered seawater with added formaldehyde brine (5% formaldehyde, final concentration) buffered with sodium tetraborate (pH 8)] were deployed on a drifting mooring in close proximity to the hydrothermal vents at 170 m and 270 m at station 5a-2019 for five days and at 270 m at station 10a-2019 for four days during the 2019 cruise, collecting sinking particulate N ("PN_{sink}"). Additionally, a long-term Technicap PPS5 trap (1 m^2 collecting area, aspect ratio of 5.3) was deployed (containing the same buffered formaldehyde brine solution described above) at station 12-2019/4-2020 at 1000 m, collecting samples every 14 days (bimonthly) for 12 months from November 2019 to October 2020. Although sediment traps are a standard tool used to capture sinking particles, uncertainties remain in their collection efficiency within the water column and between trap designs (Buesseler et al., 2007; Baker et al., 2020; Tilliette et al., 2023).

2.2 $NO_3^-+NO_2^-$ concentration and $\delta^{15}N$ analysis

For the 2019 samples, $[NO_3^-+NO_2^-]$ was determined using colorimetric analysis (Aminot and Kerouel, 2007) with a detection limit of 0.05 µM and a standard deviation (S.D.) of ± 0.1 µM. Furthermore, the $[NO_3^-+NO_2^-]$ for the 2020 samples was measured by chemiluminescence (Braman and Hendrix, 1989) using a Thermo 42i NO_x analyzer at Florida State University. Briefly, samples were injected into a heated, acidic vanadium (III) solution that reduces $NO_3^-+NO_2^-$ quantitatively to nitric oxide gas ($NO_{(g)}$). The $NO_{(g)}$ then reacts with ozone inside the analyzer to produce light, the intensity of which is quantitatively related to the amount of $NO_{(g)}$ in the sample and thus the original $[NO_3^-+NO_2^-]$. The range of detection of the instrument was adjusted according to the concentrations of the samples. Sample $[NO_3^-+NO_2^-]$ was calibrated using a standard curve that bracketed the range of samples with a lower reporting limit of 0.1 µM and an average S.D. of ± 0.1 µM.

The nitrogen (N) isotopic composition of $NO_3^-+NO_2^-$ ($\delta^{15}N_{NO3+NO2}$) was determined using the "denitrifier" method (Sigman et al., 2001; Casciotti et al., 2002; McIlvin and Casciotti, 2011; Weigand et al., 2016). This analysis was performed when sample $[NO_3^-+NO_2^-] \geq 0.3$ µM. The $\delta^{15}N_{NO3+NO2}$ values were reported when the standard deviation of replicate analyses was <0.5‰. Samples were calibrated with IAEA N3 and USGS 34 as described in McIlvin and Casciotti (2011).

2.3 Sinking particulate N flux and $\delta^{15}N$ measurements

The bulk PN_{sink} mass flux, and its associated isotopic composition, "$\delta^{15}N_{PNsink}$", collected by the sediment traps, was

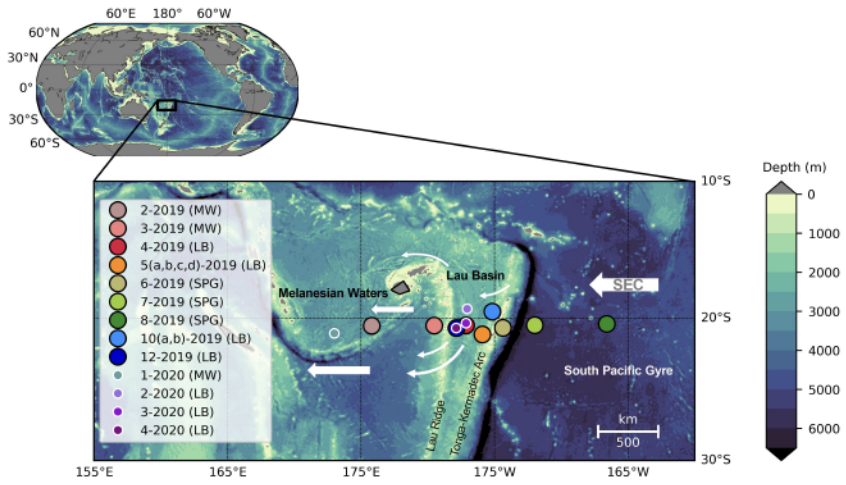

FIGURE 1
Bathymetry of the southwest Pacific region with stations from the TONGA research cruises shown in larger filled circles with black outlines (2019), and smaller filled circles with white outlines (2020); gray represents areas above sea-level. Stations 2-2019, 3-2019 and 1-2020 were sampled in Melanesian waters (MW), stations 4-2019, 5-2019, 10-2019, 12-2019, 2-2020, 3-2020, and 4-2020 were sampled in the Lau Basin (LB), and stations 6-2019, 7-2019, and 8-2019 were sampled in the South Pacific Gyre (SPG). Stations 5 (a, b, c, d)-2019 and 10 (a, b)-2019 were proximal to the shallow hydrothermal vents 'Panamax' and 'Simone', respectively. The South Equatorial Current (SEC) and branches thereof are indicated by the white arrows.

measured using an Elementar Analyser - Isotope Ratio Mass Spectrometer (EA-IRMS) at the Mediterranean Institute of Oceanography (SERCON INTEGRA 2). The Quantification Limit was 7 µg N and the precision was between ± 0.3‰ for highest masses and ± 3.5‰ for masses close to Quantification Limit (k = 2).

2.4 $\delta^{15}N$ budget calculations

A two end-member mixing model was used to evaluate the $\delta^{15}N$ budgets. This model assumes two quantitatively important "new" N sources to surface waters, subsurface $NO_3^-+NO_2^-$ and biological N_2 fixation, as well as one loss term, PN_{sink}. The isotopic composition of N_2 fixation inputs, "$\delta^{15}N_{N2\ fix}$" was assumed to be -1‰ (Hoering and Ford, 1960; Minagawa and Wada, 1986; Carpenter et al., 1997), while the $\delta^{15}N$ of subsurface $NO_3^-+NO_2^-$ and PN_{sink} were measured. The relative contribution of N_2 fixation to export production, "f_{nfix}", is calculated by the following (Knapp et al., 2018):

$$\delta^{15}N_{PNsink} = f_{nfix}(-1\%) + (1 - f_{nfix})(\delta^{15}N_{NO3+NO2}) \quad (1)$$

which can be rearranged to solve for f_{nfix}:

$$f_{nfix} = \frac{\left[(\delta^{15}N_{NO3+NO2}) - (\delta^{15}N_{PNsink})\right]}{\left[1 + (\delta^{15}N_{NO3+NO2})\right]} \quad (2)$$

The depth from which subsurface $NO_3^-+NO_2^-$ is sourced likely varies and is difficult to constrain; therefore, the short-term $\delta^{15}N$ budgets are evaluated over a range of subsurface $\delta^{15}N_{NO3+NO2}$ source values. These values include the shallowest $\delta^{15}N_{NO3+NO2}$ minima and the $\delta^{15}N_{NO3+NO2}$ of the sample collected immediately below the minima (Knapp et al., 2021). The long-term $\delta^{15}N$ budgets are evaluated using the shallowest average $\delta^{15}N_{NO3+NO2}$ minima at station 12-2019/station 4-2020 as well as the average $\delta^{15}N_{NO3+NO2}$ of South Pacific Sub-tropical Under Water (SPSTUW, 150m – 250 m depth) at station 4-2020. Note, sampling resolution at station 12-2019 did not include SPSTUW. These $\delta^{15}N_{NO3+NO2}$ end-members for the moored trap $\delta^{15}N$ bugdet were chosen to encompass the range of $NO_3^-+NO_2^-$ likely entrained to surface waters over an annual cycle (Moutin et al., 2018). This seasonality is also observed at the station ALOHA, Hawaii (Casciotti et al., 2008; Böttjer et al., 2017). Once the fraction of export supported by N_2 fixation is calculated, an N_2 fixation rate, "R_{nfix}" can be calculated by multiplying f_{nfix} by the PN_{sink} mass flux, yielding a geochemically-derived N_2 fixation rate.

2.5 Bathymetric data

Bathymetric data from the sampling region were considered to better understand the bathymetric-induced current steering as well as the proximity of the stations to the shallow hydrothermal vents. These bathymetric data were downloaded from NOAA's National Centers for Environmental Information page (https://www.ngdc.noaa.gov/mgg/global/). The ETOPO1 Global Relief Model was used with the grid version ETOPO1 Bedrock.

3 Hydrography

Water masses along the TONGA transect were identified using temperature, salinity, and potential density (σ_θ) (Figure 2) and align with those reported in Tilliette et al. (2022). Plots of the water column profiles in temperature-salinity space indicate that all stations were largely influenced by the same water masses (Figure 2), reflecting the dominance of the westward flowing SEC, which impacts waters from 400 to 1000 m across this region (Figure 1) (Talley et al., 2011; Guieu et al., 2018; Tilliette et al., 2022). The SEC divides into branches, particularly in the LB, due to the bathymetric blocking by islands and deep-sea ridges (Webb, 2000; Tilliette et al., 2022). Many of these branches in the LB are observed to have an overall southwestern trajectory before returning to a western trajectory over the center of the LB and maintaining this westward trajectory in MW (Figure 1) (Tilliette et al., 2022). Additionally, the Tonga-Kermadec Arc acts as a physical barrier to deep water masses entering the LB from the SPG, influencing circulation downstream (Tilliette et al., 2022). Surface waters across this transect were turbulent down to ~150 m with a σ_θ of 23.7 ± 0.2, temperature of 24.4 ± 0.6°C, and salinity of 35.4 ± 0.5, aligning with previous studies (Table 1) (Tilliette et al., 2022). Below that, in the thermocline and extending to ~700 m, two major water masses were present: SPSTUW and Western South Pacific Central Water (WSPCW) (Talley et al., 2011; Lehmann et al., 2018; Tilliette et al., 2022) (Figure 2) (Table 1). Across the transect, SPSTUW had an average (± 1 S.D.) σ_θ of 25.0 ± 0.2, temperature of 22.5 ± 0.8°C and was further recognized by its characteristic salinity maximum of 35.7 ± 0.1 (Talley et al., 2011; Lehmann et al., 2018; Tilliette et al., 2022) between 150 and 250 m (Table 1). Between 250 and 500 m, WSPCW was identified by a linear temperature-salinity relationship, with an average (± 1 S.D.) σ_θ of 26.4 ± 0.2, temperature of 12.6 ± 0.9°C and salinity of 34.9 ± 0.2, comparable to values reported by Lehmann et al. (2018) and Tilliette et al. (2022). Notably, between 380 and 400 m South Pacific Subtropical Mode Water (SPSTMW), a subsidiary of WSPCW, was identified by its characteristic σ_θ of 26.0 (Talley et al., 2011), with an average (± 1 S.D.) temperature of 14.9 ± 0.5°C and salinity of 35.2 ± 0.1 (Table 1). Finally, deep water masses were observed in the SPG east of the Tonga-Kermadec Arc. In particular, Antarctic Intermediate Water (AAIW) was observed at station 8-2019 and station 2-2020 between 630 and 700 m where a σ_θ of 26.9 ± 0.1 temperature of 6.5 ± 0.1°C and salinity of 34.4 ± 0.0, aligning with previous studies (Table 1) (Talley et al., 2011; Tilliette et al., 2022).

4 Results

4.1 $NO_3^-+NO_2^-$ concentration and $\delta^{15}N$

The $[NO_3^-+NO_2^-]$ in the upper 100 m of the WTSP was ≤0.1 µM except at stations influenced by the hydrothermal vents, i.e., stations 5-2019 and 10-2019, where the $[NO_3^-+NO_2^-]$ was 0.2 ± 0.0 µM to 0.7 ±

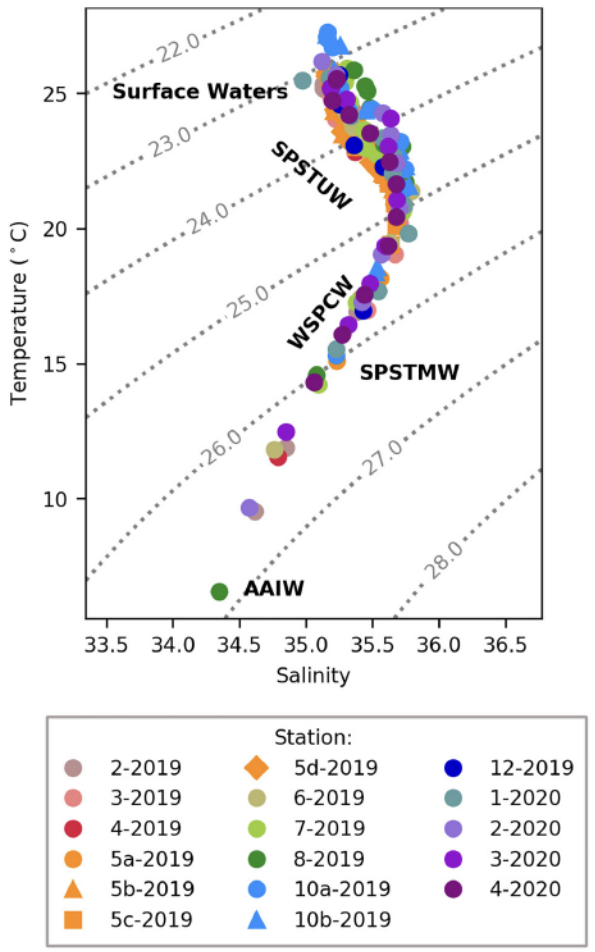

FIGURE 2
Temperature-salinity plot of samples from the 2019 and 2020 TONGA cruises as well as the prevalent water masses across the transect. The dotted grey lines indicate potential density (σ_θ) isopycnals. The water masses include surface waters, South Pacific Subtropical Under Water (SPSTUW), Western South Pacific Central Water (WSPCW), South Pacific Subtropical Mode Water (SPSTMW), a subsidiary of WSPCW and Antarctic Intermediate Water (AAIW).

0.0 µM (average ±1 S.D.) between 60 m and 100 m (Figures 3A, C). At 400 m, the $[NO_3^-+NO_2^-]$ increased to between 10 and 15 µM, corresponding to $\delta^{15}N_{NO3+NO2}$ ranging from 6 to 8‰ (Figures 3B, D). This is consistent with the presence of WSPCW (Tilliette et al., 2022) and more particularly, SPSTMW (Lehmann et al., 2018) and aligns with other studies in the region (Knapp et al., 2018). At station 8-2019, the $[NO_3^-+NO_2^-]$ increased to 26.7 µM at 630 m with a corresponding $\delta^{15}N_{NO3+NO2}$ of 6.9 ± 0.1‰ (Figures 3A, C), consistent with AAIW (Talley et al., 2011; Lehmann et al., 2018; Tilliette et al., 2022). The majority of stations within MW and the LB (i.e., stations 1-2019 to 5-2019, 10-2019, and 12-2019) had $\delta^{15}N_{NO3+NO2}$ ranging from 4 to 6‰ at 200 m, decreasing shallower in the water column to 2 to 4‰ at 150 m associated with the transition between SPSTUW and surface waters (Figures 3B, D). The SPG stations (stations 6-2019, 7-2019 and 8-2019) had an average $\delta^{15}N_{NO3+NO2}$ of 6.8 ± 0.0‰ at ~200 m characteristic of SPSTUW. This $\delta^{15}N_{NO3+NO2}$ was significantly higher than the $\delta^{15}N_{NO3+NO2}$ at 200 m in MW and LB samples, where the average $\delta^{15}N_{NO3+NO2}$ at 200 m was 5.0 ± 0.6‰ and 5.1 ± 0.6‰, respectively ($p<0.5$ and $p<0.01$, respectively, evaluated with the Kruskal-Wallis test; Kruskal and Wallis, 1952). Furthermore, the elevated $\delta^{15}N_{NO3+NO2}$ in SPG SPSTUW corresponded to significantly lower $[NO_3^-+NO_2^-]$ at 200 m (2.4 ± 0.8 µM) compared to the LB, where the average $[NO_3^-+NO_2^-]$ at 200 m was 3.3 ± 0.6 µM ($p<0.01$, Kruskal and Wallis, 1952) (Figures 3A, C). Within the surface waters (upper 150 m), the $\delta^{15}N_{NO3+NO2}$ at hydrothermal station 5-2019 was significantly lower between the four casts (5a – d), 1.8 ± 0.9‰, compared to the average $\delta^{15}N_{NO3+NO2}$ in the upper 150 m at hydrothermal station 10 (10 a, b), 4.4 ± 0.6‰ ($p<0.01$, Kruskal and Wallis, 1952) (Figures 3B, D). The lowest $\delta^{15}N_{NO3+NO2}$, 0.7 ± 0.1‰, was observed at station 5c-2019 at 100 m, above which $\delta^{15}N_{NO3+NO2}$ increased to 1.0 ± 0.0‰ at 95 m (Figures 3A, C). The $\delta^{15}N_{NO3+NO2}$ reported here for the TONGA study are publicly available (Knapp and Forrer, 2023).

4.2 PN_{sink} flux and δ15N

The PN_{sink} flux collected in the shallow short-term drifting traps was calculated to be 350 µmol N m^{-2} d^{-1} (170 m, station 5a-2019), 436 µmol N m^{-2} d^{-1} (270 m, station 5a-2019), and 693 µmol N m^{-2} d^{-1} (270 m, station 10a-2019) (Table 2). Further, the average (± 1 S.D.) $\delta^{15}N_{PNsink}$ was -0.5 ± 3.5‰ and -0.2 ± 1.9‰ at 170 m and 270 m at station 5a-2019, respectively, and -0.6 ± 2.3‰ at 270 m at station 10a-2019 (Table 2) (Figure 4). In comparison, the annual average PN_{sink} flux collected in the long-term 1000 m PPS5 moored trap at station 12-2019/4-2020 was an order of magnitude lower, 16.5 ± 14.3 µmol N m^{-2} d^{-1}, and had a higher annual mass-weighted average (± 1 S.D.) $\delta^{15}N_{PNsink}$, 3.4 ± 1.9‰, compared to the shallower, short-term traps (Table 2) (Figure 4).

The seasonal average (± 1 S.D.) PN_{sink} fluxes collected in the deep, moored trap were higher in the austral summer and autumn, at 30.9 ± 11.0 µmol N m^{-2} d^{-1} and 17.0 ± 15.4 µmol N m^{-2} d^{-1}, respectively, compared to the average austral winter and spring PN_{sink} fluxes of 8.0 ± 9.0 µmol N m^{-2} d^{-1} and 8.5 ± 8.5 µmol N m^{-2} d^{-1}, respectively (Table 2) (Figure 4). The average, mass-weighted (± 1 S.D.) summer $\delta^{15}N_{PNsink}$ from the 1000 m PPS5 moored trap, 1.5 ± 0.7‰, was lower than the wintertime average of 5.9 ± 1.1‰, while the average (± 1 S.D.) spring and autumn mass-weighted $\delta^{15}N_{PNsink}$, 2.9 ± 0.5‰ and 3.3 ± 1.7‰, respectively, were intermediate between summer and winter values.

4.3 Results of the $\delta^{15}N$ budget

The $\delta^{15}N$ budget described above compares the $\delta^{15}N$ of the primary form of N exported from the euphotic zone, $\delta^{15}N_{PNsink}$, with the $\delta^{15}N$ of the two input terms, subsurface $NO_3^-+NO_2^-$ and N_2 fixation. This provides a geochemically-derived estimate of the fractional contribution of N_2 fixation to export production (f_{nfix}) as well as rate of N_2 fixation (R_{nfix}). Given that the subsurface $\delta^{15}N_{NO3+NO2}$ source is difficult to constrain, we evaluate the shallow $\delta^{15}N$ budgets using the shallowest subsurface $\delta^{15}N_{NO3+NO2}$ minima as well as the sample immediately below the minima (Knapp et al., 2021), while the $\delta^{15}N$ budget using the deep trap PN_{sink} flux uses the average subsurface

TABLE 1 Water masses identified from the 2019 and 2020 TONGA cruises and their average (± 1 S.D.) hydrographic and $NO_3^-+NO_2^-$ properties and number (n) of samples from each water mass.

Water Mass	Depth (m)	Temperature (°C)	Salinity	σ_θ	$[NO_3^-+NO_2^-]$ µM	$\delta^{15}N_{NO3+NO2}$ (‰ vs. N_2 in air)
Surface waters (97)	0 – 150	24.4 ± 0.6[1]	35.4 ± 0.5[1]	23.7 ± 0.2	0.2 ± 0.2[1]	2.4 ± 1.5[4] 4.3 ± 1.7[5]
SPSTUW (38)	150 – 250	22.5 ± 0.8[1,3]	35.7 ± 0.1[1,3]	25.0 ± 0.2	2.4 ± 0.8	4.9 ± 1.4
WSPCW (30)	250 – 550	12.6 ± 0.9[1,2]	34.9 ± 0.2[1,2]	26.4 ± 0.2[2]	7.8 ± 2.5[1]	7.0 ± 0.7[2]
SPSTMW (4)	380 – 400	14.9 ± 0.5[3]	35.2 ± 0.1[3]	26.0 ± 0.0[3]	9.0 ± 0.5	7.4 ± 0.4
AAIW (2)	> 600	6.5 ± 0.1	34.4 ± 0.0[1,3]	26.9 ± 0.1[2,3]	26.7 ± 1.2[1]*	6.9 ± 0.1[2]*

[1]Tilliette et al., 2022
[2]Lehmann et al., 2018
[3]Talley et al., 2011
[4] Average for hydrothermal vent stations only (station 5-2019 and station 10-2019).
[5] Average for all non-hydrothermal vent stations (i.e., all stations except station 5-2019 and station 10-2019).
*n = 1 for this measurement.
These data align with the studies indicated in superscript.

$\delta^{15}N_{NO3+NO2}$ minima at station 12-2019/4-2020 and the average SPSTUW $\delta^{15}N_{NO3+NO2}$ at station 4-2020. At the shallow trap stations in close proximity to the hydrothermal vents, the subsurface $\delta^{15}N_{NO3+NO2}$ ranged from 1.2 to 2.2‰ and 3.6 to 4.7‰ at stations 5-2019 and 10-2019, respectively, while at the deep mooring (station 12-2019/4-2020) the average subsurface $\delta^{15}N_{NO3+NO2}$ minima and SPSTUW $\delta^{15}N_{NO3+NO2}$ were 2.4‰ and 4.6‰, respectively (Table 2). Additional uncertainty in the $\delta^{15}N$ budgets includes the standard deviation of the $\delta^{15}N_{PNsink}$ analysis (Table 2). The $\delta^{15}N$ value for N_2 fixation, ($\delta^{15}N_{Nfix}$) of -1‰ is based on literature reports of diazotrophic

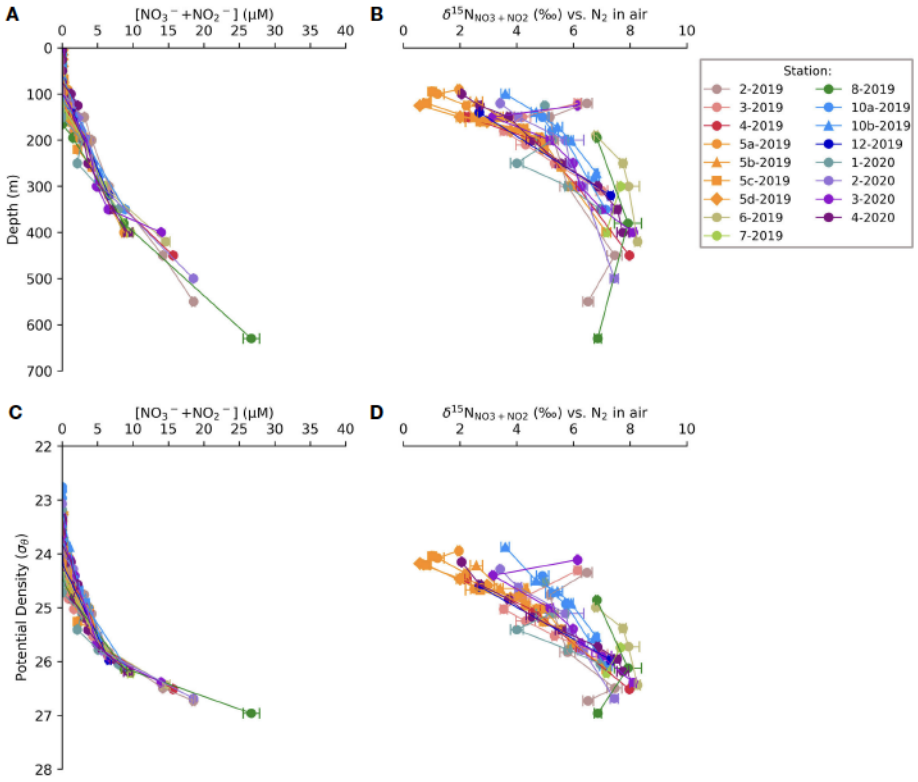

FIGURE 3
Water column profiles of $[NO_3^-+NO_2^-]$ and $\delta^{15}N_{NO3+NO2}$ vs. depth of samples from the 2019 and 2020 TONGA cruises **(A, B)** and vs. potential density **(C, D)**. Error bars represent ±1 S.D. and are often smaller than the symbol size.

biomass $\delta^{15}N$ (Hoering and Ford, 1960; Minagawa and Wada, 1986; Carpenter et al., 1997) (Table 2). Comparing these values with the $\delta^{15}N_{PNsink}$, we calculate that at station 5-2019, the f_{nfix} ranged from 77 to 84 ± 159% for the 170 m trap, while the f_{nfix} ranged from 64 to 76 ± 86% at the 270 m trap (Table 2). At station 10-2019, the f_{nfix} at the 270 m trap ranged from 90 to 92 ± 50% (Table 2). We further calculate a geochemically derived R_{nfix} of 282 ± 550 μmol N m^{-2} d^{-1} and 331 ± 375 μmol N m^{-2} d^{-1} for the 170 m and 270 m traps deployed at station 5-2019, respectively, and 638 ± 347 μmol N m^{-2} d^{-1} for the 270 m trap deployed at station 10-2019 (Table 2). The $\delta^{15}N$ budget calculated for the moored trap at station 12-2019/4-2020 (note that the trap is deeper, i.e. 1000 m instead of 170 – 270 m for the drifting ones) yielded a mass-weighted f_{nfix} of 12 to 64 ± 29% (average = 42 ± 13%) for the summer, while the spring and autumn had similar but lower mass-weighted f_{nfix} of 0 to 37 ± 21% (average = 0 ± 29%) and 0 to 43 ± 69% (average = 12 ± 36%), respectively, and winter had a mass-weighted f_{nfix} of 0 ± 18%.

TABLE 2 The mass and isotopic composition of the sinking particulate N (PN_{sink}) flux captured in the short-term PIT and long-term PPS5 traps, and results of the $\delta^{15}N$ budgets.

	Stn.	Lon.	Trap depth (m)	Time (days)*	Season[1]	Av. PN_{sink} flux (μmol N m^{-2} d^{-1})[2]	Av. $\delta^{15}N_{PNsink}$[2] (‰)	$\delta^{15}N_{NO3+NO2}$ end-member range[3] (‰)	f_{nfix}[4] (%)	R_{nfix}[4] (μmol N m^{-2} d^{-1})	Bottle-based av. N_2 fix rate[2] (μmol N m^{-2} d^{-1})
TONGA (this study)	5-2019 (LB)	175.9° W	170	5	Late Spring	350	-0.5 ± 3.5	1.2 – 2.2	77 to 84 ± 159	282 ± 550	1942 ± 1212[6]
	5-2019 (LB)	175.9° W	270	5	Late Spring	436	-0.2 ± 1.9	1.2 – 2.2	64 to 76 ± 86	331 ± 375	1942 ± 1212[6]
	10-2019 (LB)	175.2° W	270	4	Late Spring	693	-0.6 ± 2.3	3.6 – 4.7	90 to 92 ± 50	638 ± 347	2047 ± 566[6]
	12-2019/4-2020[5] (LB)	177.9° W	1000	360	Spring	8.5 ± 8.5	2.9 ± 0.5[9]	2.4[7] – 4.6[8]	0 to 37 ± 21[9]	-[10]	-[10]
					Summer	30.9 ± 11.0	1.5 ± 0.7[9]		12 to 64 ± 29[9]	-[10]	-[10]
					Autumn	17.0 ± 15.4	3.3 ± 1.7[9]		0 to 43 ± 69[9]	-[10]	-[10]
					Winter	8.0 ± 9.0	5.9 ± 1.1[9]		0 ± 18[9]	-[10]	-[10]
OUTPACE (Knapp et al., 2018)	A (MW)	163.6 °E	150	5	Late summer	303	0.6 ± 1	7.0 – 8.4	80 to 83 ± 13	254 ± 50	593 ± 5[11]
	B (SPG)	170.7° W	150	5	Autumn	30	3.1 ± 1	7.2 – 8.3	50 to 56 ± 12	16 ± 6	706 ± 302[11]
	C (SPG)	165.8° W	150	5	Autumn	47	7.7 ± 1	7.0 – 8.4	0 to 8 ± 11	5 ± 5	59 ± 16[11]

[1] Austral seasons divided into: Spring (September, October, November), Summer (December, January, February), Autumn (March, April, May), Winter (June, July, August).
[2] average ± 1 S.D.
[3] Subsurface $\delta^{15}N_{NO3+NO2}$.
[4] See Methods section 2.6.
[5] Samples collected bimonthly, then seasonally averaged.
[6] Lory et al., 2023.
[7] Shallow subsurface $\delta^{15}N_{NO3+NO2}$ minima end-member for station 12-2019 and 4-2020.
[8] Average SPSTUW $\delta^{15}N_{NO3+NO2}$ end-member at station 4-2020. Note, sampling resolution at station 12-2019 did not include SPSTUW.
[9] Mass-weighted average values for each season.
[10] No data.
[11] Caffin et al., 2018

The table includes the range in the $\delta^{15}N_{NO3+NO2}$ end-member, fraction of export production supported by N_2 fixation ("f_{nfix}") and N_2 fixation rate determined by multiplying the PN_{sink} flux by f_{nfix} for the TONGA (this study) and OUTPACE (Knapp et al., 2018) projects. Uncertainty in f_{nfix} and R_{nfix} reflects both the range in $\delta^{15}N_{NO3+NO2}$ end-member as well as the standard deviation of the PN_{sink} $\delta^{15}N$ measurements.
*Trap deployment time.

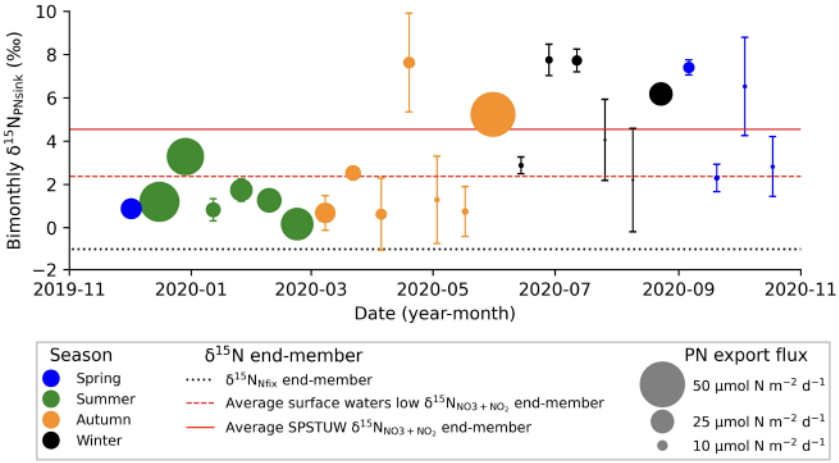

FIGURE 4
Bimonthly measurements of PN_{sink} flux and $\delta^{15}N_{PNsink}$ from the 1000 m trap deployed at station 12-2019/station 4-2020 between November 2019 to October 2020. Circle color corresponds to the season when the majority of the PN_{sink} was collected over bimonthly sampling intervals and circle size corresponds to PN_{sink} flux magnitude (µmol N m^{-2} d^{-1}). Each measurement is plotted at the end date of the two-week sampling interval. The $\delta^{15}N_{Nfix}$ end-member (-1‰) is represented by the dotted black line and the low $\delta^{15}N_{NO3+NO2}$ end-member at station 12-2019 and 4-2020 (2.4‰) and average SPSTUW $\delta^{15}N_{NO3+NO2}$ end-member at station 4-2020 (4.6‰) are represented by the dashed and solid lines, respectively. Data available in Supplementary Table S1.

These f_{nfix} values indicate that the highest contribution of N_2 fixation to export production collected at 1000 m was during the summer, followed by autumn and spring. Due to significant PN_{sink} flux attenuation with depth (Martin et al., 1987), we do not calculate a R_{nfix} for the moored trap data.

5 Discussion

5.1 TONGA δ^{15}N budgets reflect high rates of N_2 fixation in the WTSP

The results of the short-term δ^{15}N budgets suggest that N_2 fixation rates were high (282 to 638 µmol N m^{-2} d^{-1}) near the hydrothermal vents at the time of the 2019 cruise. While there are notable differences in the magnitude of these geochemically-derived N_2 fixation rates and the bottle-based $^{15}N_2$ uptake rates reported by Lory et al., 2023, we consider these results to be broadly consistent with one another, as well as consistent with estimates of diazotroph abundance measured contemporaneously (Bonnet et al., 2023b). Specifically, bottle-based $^{15}N_2$ uptake rates were 3 to 7 times higher than the R_{nfix} estimated from the δ^{15}N budget (Table 2); however, both rate estimates are at the upper-end typically reported by each technique (Gruber, 2004; Capone et al., 2005; Casciotti et al., 2008; Luo et al., 2012; Knapp et al., 2016a) and align with previous work from the region (Montoya et al., 2004; Berthelot et al., 2017; Bonnet et al., 2017; Knapp et al., 2018; Shao et al., 2023). Prior work investigating N_2 fixation's contribution to export production has attributed discrepancies between these two metrics to potential sediment trap under collection of exported material (Knapp et al., 2016a; Böttjer et al., 2017, Knapp et al., 2018), alternate sources of fixed N to the euphotic zone including horizontal advection (Böttjer et al., 2017), phytoplankton bloom stage as well as temporal delay between organic matter formation and capture by the sediment trap (de Verneil et al., 2017; Caffin et al., 2018; Knapp et al., 2018), and bottle-based $^{15}N_2$ incubations with their associated methodological considerations (i.e., bottle effects) (White et al., 2020). Additionally, our δ^{15}N budgets should be considered a lower bound for estimated N_2 fixation rates because of the mixing-model's inherent assumption that the only fate of newly fixed N is to be balanced by the sinking flux, and that no newly fixed N is released to the dissolved pool, which is likley unrealistic (Capone et al., 1994; Glibert & Bronk, 1994; Mulholland and Capone, 2004; Bonnet et al., 2016; Knapp et al., 2016b). Further, the trap depth used here, 170 m, is below the base of the mixed layer, and thus underestimates new/export production. While euphotic zone nitrification is a source of low-$\delta^{15}N_{NO3}$ that could lead to an overestimation of N_2 fixation supported export production, rates of euphotic zone nitrification from this and other similar oligotrophic regions are low (<10 nmol L^{-1} d^{-1}) (Smith et al., 2014; Raes et al., 2020) compared to the very high rates of N_2 fixation using multiple metrics in this study. This therefore suggests that N_2 fixation is the dominant mechanism generating the low-$\delta^{15}N_{PNSink}$ signal observed.

Regardless of the mechanism(s) driving these discrepancies, both the δ^{15}N budget and $^{15}N_2$ uptake rate estimates are also consistent with the elevated diazotroph abundances (Bonnet et al., 2023a; Lory et al., 2023) observed on the 2019 TONGA cruise (Figure 5). Here we compare averages of biological and geochemical metrics associated with N_2 fixation for the three hydrographic regions, MW, the LB, and the SPG (defined in Section 2.1). While results from the qPCR analysis targeting *nifH* genes indicate that *Trichodesmium* spp. and UCYN-A dominated the diazotroph assemblage in the upper 50 m across the TONGA transect, *Trichodesmium* spp. were most abundant in the LB near the hydrothermal vents (average 1.0x10^7 gene copies L^{-1}), followed by UCYN-A (average 3.0x10^6 gene copies L^{-1}) (Figures 5A, B). These

exceptionally high abundances of *Trichodesmium* spp. and UCYN-A were on the order of one to four times higher than previous studies (e.g., Zehr & Turner, 2001; Moisander et al., 2010; Turk-Kubo et al., 2012; Moisander et al., 2014; Benavides et al., 2018; Benavides et al., 2020; Confesor et al., 2022). Notably, the highest regionally-averaged, trapezoidally-integrated upper 50 m $^{15}N_2$ uptake rates were found in the LB (1038 ± 600 μmol N m^{-2} d^{-1}), where *Trichodesmium* spp. were most abundant and where the lowest regionally-averaged $\delta^{15}N_{NO3+NO2}$ subsurface minima of 2.8 ± 1.5‰ (Figure 5F) was observed between 100 and 200 m. This underscores the potential significance of *Trichodesmium* spp. supporting N_2 fixation near the hydrothermal vents. UCYN-A was the dominant diazotroph in the upper 50 m in MW and the SPG, with regional averages of 2.5x10^8 gene copies L^{-1} and 3.1x10^8 gene copies L^{-1}, respectively, followed by *Trichodesmium* spp., with regional averages of 3.0x10^5 and 3.7x10^5 gene copies L^{-1}, respectively. Average abundances of UCYN-B (2.6x10^4 to 3.2x10^5 gene copies L^{-1}), UCYN-C (4.3x10^1 to 1.7x10^2 gene copies L^{-1}) and Gamma proteobacteria (5.4x10^3 to 9.9x10^3 gene copies L^{-1}) remained comparatively low across the transect (Figures 5C–E), but were similar in magnitude to previous studies in the region (Moisander et al., 2014; Benavides et al., 2018; Benavides et al., 2020). Although UCYN-A have extremely high gene abundances and dominate the upper 50 m in MW and the SPG, the trapezoidally-integrated upper 50 m $^{15}N_2$ uptake rates were lower than in the LB, 713 ± 691 and 537 ± 629 μmol N m^{-2} d^{-1}, respectively, and were associated with a higher regional average $\delta^{15}N_{NO3+NO2}$ subsurface minima of 4.4 ± 1.2‰ and 5.5 ± 1.9‰, respectively, observed between 100 to 200 m (Figure 5F). While care should be taken when relating *nifH* gene copies to diazotroph biomass, these gene copy abundances broadly correspond to elevated diazotroph abundances (Meiler et al., 2022) and confirm the significance of diazotrophy in the region.

5.2 N_2 fixation is an important source of N supporting export production in the WTSP

The agreement between the geochemically-derived N_2 fixation rates, $^{15}N_2$ uptake rates and diazotroph abundances together indicate that export production in the WTSP at the time of this study was driven by N_2 fixation (Bonnet et al., 2023b). This is in contrast to prior work in other oligotrophic regions where the majority of export was supported by subsurface NO_3^-, even when N_2 fixation inputs were high (Casciotti et al., 2008; Bourbonnais et al., 2009; White et al., 2013; Böttjer et al., 2017). The shallow sediment traps deployed for the TONGA project indicate that N_2 fixation supports a majority of export production (f_{nfix} = 64 to 92%) near the hydrothermal vents, at least in the late spring (Table 2; Figures 6A, B). These f_{nfix} values are similar to those calculated from the previous OUTPACE campaign during the late summer/early autumn in MW (station A, 80 to 83 ± 13%), and near the Tonga-

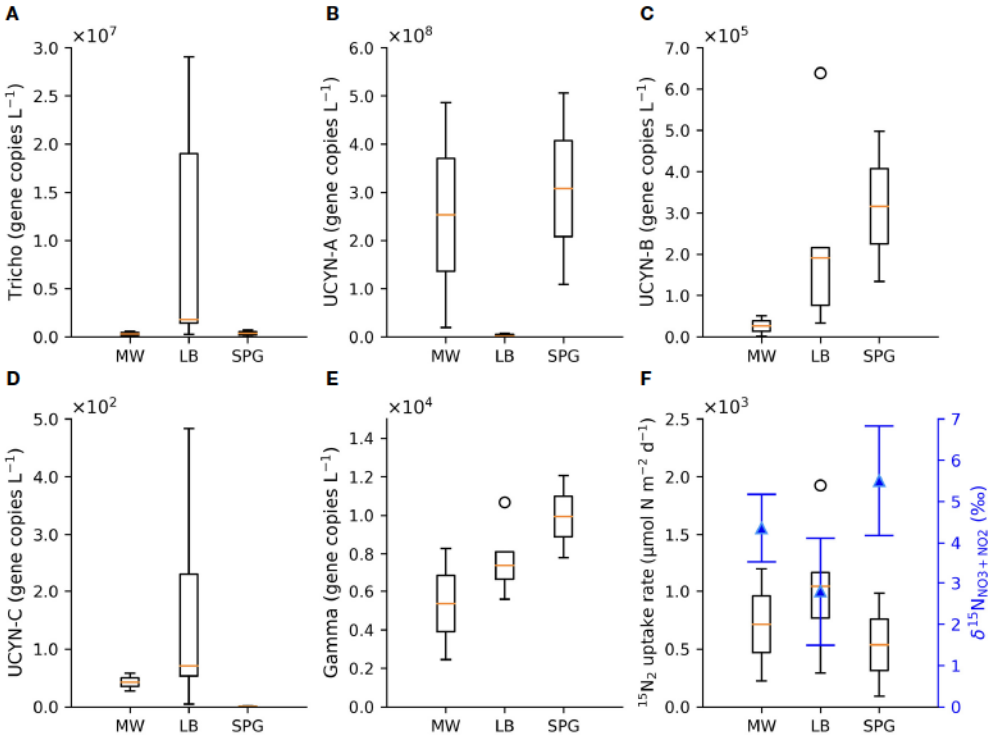

FIGURE 5
Box plots of the upper 50 m *nifH* gene abundances (gene copies L^{-1}) from Bonnet et al., 2023a and Lory et al., 2023 for the hydrographic regions of MW, the LB and the SPG for **(A)** *Trichodesmium* spp., **(B)** UCYN-A, **(C)** UCYN-B, **(D)** UCYN-C, and **(E)** Gamma proteobacteria, as well as (F) box plots of the regional average, trapezoidally-integrated upper 50 m $^{15}N_2$ fixation rates from Lory et al., 2023, with the corresponding regional average 90 to 195 m $\delta^{15}N_{NO3+NO2}$ (blue triangles). The open circles associated with the box plots indicate outliers.

Kermadec Arc (station B, 50 to 56 ± 12%) (Table 2; Figure 6C) (Knapp et al., 2018). The high f_{nfix} values reported here from the short-term traps deployed at TONGA Stations 5 and 10 replicate a geochemical signature that has not been observed outside of the WTSP, underscoring the significance of N_2 fixation regionally (Bonnet et al., 2023b). We also emphasize the potential for the f_{nfix} from our $\delta^{15}N$ budgets to underestimate the importance of N_2 fixation to export due to the mixing-model's inherent assumption that the only fate of newly fixed N is the PN_{sink} flux captured by the sediment traps, as opposed to being released and persisting as dissolved organic nitrogen (Capone et al., 1994; Glibert and Bronk, 1994).

While the results of the short-term $\delta^{15}N$ budgets from both the TONGA and OUTPACE campaigns found that N_2 fixation supports the majority of export production in the late spring, late summer, and early autumn in the LB and MW, we also consider the $\delta^{15}N_{PNsink}$ collected in the deep, moored trap at station 12-2019/4-2020 in the LB to evaluate this trend over an annual cycle (Figure 4). Unsurprisingly, the mass flux collected in the shallower, short-term PIT traps was higher and the $\delta^{15}N_{PNsink}$ was lower than that collected in the deeper, moored trap. However, we note that the moored trap was deployed ~200 km west of the shallow traps and hydrothermal vents (Table 2) (Figures 1, 4), and the conical shape of the PPS5 has been observed to undersample (Baker et al., 2020; Tilliette et al., 2023). The $\delta^{15}N_{PNsink}$ in the shallow PIT traps collected in the late spring at stations 5-2019 and 10-2019 ranged from -0.2 to -0.6‰ compared to a seasonal average $\delta^{15}N_{PNsink}$ of 2.9 ± 0.5‰ and 1.5 ± 0.7‰ observed in the moored PPS5 trap during the spring and summer, respectively. We expect that the higher $\delta^{15}N_{PNsink}$ found in the deeper moored trap likely resulted from the collection of PN_{sink} from a larger surface area than the shallow short-term traps, where export production may have been supported by a mixture of N sources with higher $\delta^{15}N$ (Siegel and Deuser, 1997; Siegel et al., 2008). Additionally, horizontal advection of particles generated at locations not impacted by the shallow hydrothermal vents potentially decouples the euphotic zone diazotrophic abundance and/or importance from the PN collected in the moored trap (Waniek et al., 2000). Indeed, the exported material in the deep trap was observed to be compositionally different from that captured in the shallow, short-term traps, where the hydrothermal signature of the particles was less evident due to organic matter remineralization while being transported to depth (Tilliette et al., 2023). The associated distance and time components of sinking PN to the deep trap potentially underestimates the importance of N_2 fixation to export production. Similar flux and isotopic composition offsets have been observed between shallow and deep sediment traps in the ETSP (Berelson et al., 2015; Knapp et al., 2016a; Tilliette et al., 2023).

Since aerosol inputs to this region are minimal (Guieu et al., 2018), we expect that the seasonal variability of $\delta^{15}N_{PNsink}$ in the deep, moored trap reflects shifts in the importance of N_2 fixation and subsurface NO_3^- for supporting export production over seasonal timescales. In the deep trap, annual PN_{sink} fluxes peaked in the summer (30.9 ± 11.0 µmol N m^{-2} d^{-1}), coinciding with the lowest average mass-weighted $\delta^{15}N_{PNsink}$, 1.5 ± 0.7‰, while the lowest PN_{sink} fluxes were observed in the winter (8.0 ± 9.0 µmol N m^{-2} d^{-1}) and coincided with the highest average mass-weighted $\delta^{15}N_{PNsink}$, 5.9 ± 1.1‰, indicating that isotopically distinct N sources support export seasonally. Since there are steep gradients in both $[NO_3^-+NO_2^-]$ and $\delta^{15}N_{NO3+NO2}$ with depth (Figures 3, 6), a higher winter $\delta^{15}N_{PNsink}$ may reflect entrainment of a deeper $NO_3^-+NO_2^-$ source (likely SPSTUW) with a higher $\delta^{15}N_{NO3+NO2}$ due to winter mixing (Moutin et al., 2018). The net effect of a higher subsurface $\delta^{15}N_{NO3+NO2}$ end-member would be to raise the estimated f_{nfix} (Table 2) (Böttjer et al., 2017). As a result, the mass-weighted seasonal f_{nfix} values for the deep trap range from 12 to 64 ± 29% in the summer and 0 ± 18% in the winter, describing a largely N_2 fixation supported export system in the summer. Further, since the majority of annual export is focused in the summer, and was supported by low-$\delta^{15}N$ N sources, we attribute an important fraction of annual export production and deep (>1000 m) long-term C sequestration to N_2 fixation at station 12-2019/4-2020 (Figure 4; Table 2).

Considering the elevated chlorophyll *a* concentrations observed over a large area in this region ranging up to 360,000 km^2 (Bonnet et al., 2023b), and given the high R_{nfix} and f_{nfix} values estimated at station 5a-2019 and 10a-2019, along with the large fraction of N_2 fixation supported export production at station 12-2019/4-2020 over an annual timescale, the otherwise oligotrophic WTSP appears to be biogeochemically unique where N_2 fixation supports a large fraction of annual export production as a result of the influence of shallow hydrothermal vents. The significance of these regional N_2 fixation inputs in the WTSP are further pronounced in the gradients of water column $\delta^{15}N_{NO3+NO2}$ both zonally as well as with depth (Figures 3, 6). In particular, $\delta^{15}N_{NO3+NO2}$ between 150 and 400 m decreases from east to west (SPG to MW) across the zonal transect, and also decreases from ~400 m to shallower depths. These isotopic gradients reflect the accumulation of low-$\delta^{15}N$ N inputs in the upper thermocline to the west along this transect that are presumably associated with the remineralization of diazotrophic inputs (Casciotti et al., 2008; Knapp et al., 2008). This accumulation of low-$\delta^{15}N_{NO3+NO2}$ in the upper 400 m of the WTSP erodes the elevated $\delta^{15}N_{NO3+NO2}$ originating from dissimilatory NO_3^- reduction occurring in the oxygen deficient zones of the ETSP (Bourbonnais et al., 2015; Peters et al., 2018; Casciotti et al., 2013), a geochemical signature that reflects basin-scale compensation of N losses in the east with N inputs in the west that is consistent with peloceanographic records (Brandes and Devol, 2002; Deutsch et al., 2004; Weber and Deutsch, 2014; Knapp et al., 2018).

6 Conclusions

Here we report results of $\delta^{15}N$ budgets that compare subsurface $\delta^{15}N_{NO3+NO2}$ with the $\delta^{15}N_{PNsink}$ captured in short-term, shallow (170 and 270 m) PIT deployed near the hydrothermal vents of the Tonga-Kermadec Arc and long-term, deep (1000 m) moored PPS5 sediment

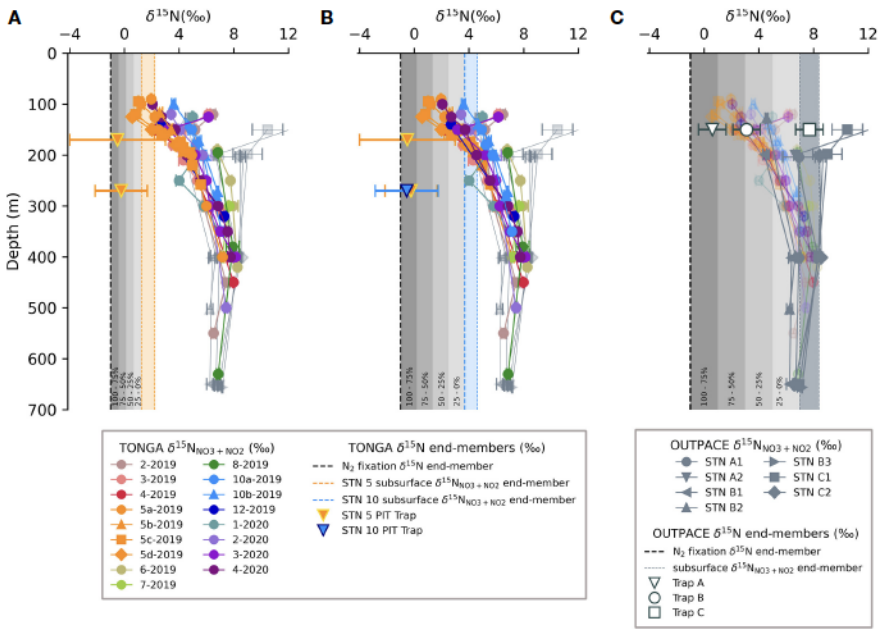

FIGURE 6
The fraction of N_2 fixation-supported export production in the austral spring at **(A)** TONGA station 5-2019, and, **(B)** TONGA station 10-2019, compared with **(C)** results from the austral late summer/early autumn at OUTPACE stations(**A-C**) Each panel includes water column profiles of $\delta^{15}N_{NO3+NO2}$ for samples from the 2019 and 2020 TONGA cruises in color and the OUTPACE cruise in grey and the associated $\delta^{15}N$ budget terms, including the sediment trap $\delta^{15}N_{PNsink}$ (inverted triangles and open circle and square), the $\delta^{15}N_{Nfix}$ (vertical dashed line) and ranges in subsurface $\delta^{15}N_{NO3+NO2}$, which are represented by the orange shaded region in **(A)**, blue shaded region in **(B)**, and steel-grey shaded region in **(C)** (Table 2). The fractional contribution of N_2 fixation to export production is indicated by the grey shading and the corresponding fraction is indicated along the bottom of each panel.

traps deployed ~200 km west of the Arc. These results are evaluated in the context of $^{15}N_2$ uptake rates (Lory et al., 2023) and *nifH* gene abundances (Bonnet et al., 2023b) collected contemporaneously, as well as with prior work from the region (Knapp et al., 2018). Results from the short-term, shallow $\delta^{15}N$ budgets indicate that N_2 fixation supports the majority, 64 to 92%, of export in late spring in the Lau Basin, while the mass-weighted, seasonally-averaged $\delta^{15}N$ budgets from deeper traps suggest that N_2 fixation supports 12 to 64% of export production and thus long-term C sequestration in the summer when the highest PN_{sink} fluxes are observed. As the seasons progress into winter, export production becomes increasingly supported by subsurface NO_3^-. The observations from this cruise as well as from the OUTPACE study (Knapp et al., 2018) are in contrast to other regions explored so far, where even significant N_2 fixation inputs do not support the majority of export (Casciotti et al., 2008; Bourbonnais et al., 2009; Böttjer et al., 2017), underscoring the significance of diazotrophy in the WTSP. While diazotroph abundance was high across the transect, *Trichodesmium* spp. *nifH* gene copies were highest in the vicinity of the hydrothermal vents, which appear shallow enough to meet the considerable Fe demands of primary productivity in general (Tilliette et al., 2022), and N_2 fixation in particular, in the region (Bonnet et al., 2023b), highlighting the sensitivity of N_2 fixation to Fe availability. These results suggest that the significant N_2 fixation inputs to the WTSP in the late spring, summer, and early autumn work to lower the elevated upper thermocline $\delta^{15}N_{NO3+NO2}$ originating from dissimilatory NO_3^- reduction in the oxygen deficient zones of the Eastern Tropical South Pacific.

Data availability statement

The datasets presented in this study can be found in online repositories. The names of the repository/repositories and accession number(s) can be found in the article/Supplementary Material.

Author contributions

SB, CG, and AK designed the study. SB and CG carried out the sampling. HF and RT carried out the $\delta^{15}N_{NO3+NO2}$ sample analysis and data aqusition. SB and OG carried out the $\delta^{15}N_{PNsink}$ sample analysis and data aqusition. HF and AK wrote the first manuscript draft, which was then revised by all authors. All authors contributed to the article and approved the submitted version.

Funding

The author(s) declare financial support was received for the research, authorship, and/or publication of this article. This research is a contribution to the TONGA project (Shallow hydroThermal sOurces of trace elemeNts: potential impacts on biological productivity and the biological carbon pump; TONGA cruise https://doi.org/10.17600/18000884) funded by the Agence Nationale de la Recherche (grant TONGA ANR-18- CE01-0016), the LEFE-CyBER

program (CNRS-INSU), the A-Midex foundation, the TGIR Flotte océanographique française, the Institut de Recherche pour le Développement (IRD). HF acknowledges funding from the Winchester Fund at Florida State University's EOAS Department. AK acknowledges NSF OCE-1829797 for supporting the nitrate isotopic analyses.

Acknowledgments

The authors warmly thank the captain and crew of the R/V L'Atalante and R/V Alis (both TGIR Flotte, operated by IFREMER) for outstanding shipboard operations. Vincent Taillandier and Nagib Bhairy are thanked for the CTD rosettes management, and data processing, Sandra Nunige for nutrient analyses of the 2019 samples, Mary Dennis for her assistance with the 'denitrifier method' at Florida State University, Caroline Lory for her assistance with the $^{15}N_2$ fixation experiments and data aqusition and Nathalie Leblond (Cellule Piège INSU) for the treatment/splitting of the moored trap.

Conflict of interest

The authors declare that the research was conducted in the absence of any commercial or financial relationships that could be construed as a potential conflict of interest.

Publisher's note

Supplementary material

The Supplementary Material for this article can be found online at: https://www.frontiersin.org/articles/10.3389/fmars.2023.1249115/full#supplementary-material

References

Altabet, M. A. (1988). Variations in nitrogen isotopic composition between sinking and suspended particles: implications for nitrogen cycling and particle transformation in the open ocean', Deep Sea Research Part A. *Oceanographic Res. Papers* 35.4), 535–554. doi: 10.1016/0198-0149(88)90130-6

Aminot, A., and Kerouel, R. (2007). Dosage automatique des nutriments dans les eaux marines: méthodes en flux continu, Ifremer, Plouzané.

Baker, C. A., Estapa, M. L., Iversen, M., and Lampitt Buesseler, R. K. (2020). Are all sediment traps created equal? An intercomparison study of carbon export methodologies at the PAP-SO site. *Prog. Oceanography* 184, 102317. doi: 10.1016/j.pocean.2020.102317

Benavides, M., Martias, C., Elifantz, H., Berman-Frank, I., Dupouy, C., and Bonnet, S. (2018). Dissolved organic matter influences N2 fixation in the New Caledonian lagoon (Western tropical south pacific). *Front. Mar. Sci.* 5, 89. doi: 10.3389/fmars.2018.00089

Benavides, M., Duhamel, S., Van Wambeke, F., Shoemaker, K. M., Moisander, P. H., Salamon, E., et al. (2020). Dissolved organic matter stimulates N2 fixation and *nifH* gene expression in *Trichodesmium*. *FEMS Microbiol. Lett.* 367 (4), fnaa034. doi: 10.1093/femsle/fnaa034

Berelson, W. M., Haskell, W. Z., Prokopenko, M., Knapp, A. N., Hammond, D. E., Rollins, N., et al. (2015). Biogenic particle flux and benthic remineralization in the Eastern Tropical South Pacific. *Deep Sea Res. Part I: Oceanographic Res. Papers* 99, 23–34. doi: 10.1016/j.dsr.2014.12.006

Berman-Frank, I., Cullen, J. T., Shaked, Y., Sherrell, R. M., and Falkowski, P. G. (2001). Iron availability, cellular iron quotas, and nitrogen fixation in *Trichodesmium*. *Limnology Oceanography* 46 (6), 1249–1260. doi: 10.4319/lo.2001.46.6.1249

Berthelot, H., Benavides, M., Moisander, P. H., Grosso, O., and Bonnet, S. (2017). High-nitrogen fixation rates in the particulate and dissolved pools in the Western Tropical Pacific (Solomon and Bismarck Seas). *Geophysical Res. Lett.* 44 (16), 8414–8423. doi: 10.1002/2017GL073856

Bonnet, S., Biegala, I. C., Dutrieux, P., Slemons, L. O., and Capone, D. G. (2009). Nitrogen fixation in the western equatorial Pacific: Rates, diazotrophic cyanobacterial size class distribution, and biogeochemical significance: N_2 FIXATION IN THE EQUATORIAL PACIFIC. *Global Biogeochemical Cycles* 23 (3). doi: 10.1029/2008GB003439

Bonnet, S., Berthelot, H., Turk-Kubo, K., Fawcett, S., Rahav, E., L'Helguen, S., et al. (2016). Dynamics of N_2 fixation and fate of diazotroph-derived nitrogen in a low-nutrient, low-chlorophyll ecosystem: results from the VAHINE mesocosm experiment (New Caledonia). *Biogeosciences* 13 (9), 2653–2673. doi: 10.5194/bg-13-2653-2016

Bonnet, S., Caffin, M., Berthelot, H., and Moutin, T. (2017). Hot spot of N_2 fixation in the western tropical South Pacific pleads for a spatial decoupling between N_2 fixation and denitrification. *Proc. Natl. Acad. Sci.* 114 (14). doi: 10.1073/pnas.1619514114

Bonnet, S., Benavides, M., Le Moigne, F. A. C., Camps, M., Torremocha, A., Grosso, O., et al. (2023a). Diazotrophs are overlooked contributors to carbon and nitrogen export to the deep ocean. *ISME J.* 17 (1), 47–58. doi: 10.1038/s41396-022-01319-3

Bonnet, S., Guieu, C., Taillandier, V., Boulart, C., Bouruet-Aubertot, P., Gazeau, F., et al. (2023b). Natural iron fertilization by shallow hydrothermal sources fuels diazotroph blooms in the ocean. *Science* 380 (6647), 812–817. doi: 10.1126/science.abq4654

Böttjer, D., Dore, J. E., Karl, D. M., Letelier, R. M., Mahaffey, C., Wilson, S. T., et al. (2017). Temporal variability of nitrogen fixation and particulate nitrogen export at Station ALOHA. *Limnology Oceanography* 62 (1), 200–216. doi: 10.1002/lno.10386

Bourbonnais, A., Lehmann, M. F., Waniek, J. J., and Schulz-Bull, D. E. (2009). Nitrate isotope anomalies reflect N_2 fixation in the Azores Front region (subtropical NE Atlantic). *J. Geophysical Res.* 114 (C3), C03003. doi: 10.1029/2007JC004617

Bourbonnais, A., Altabet, M. A., Charoenpong, C. N., Larkum, J., Hu, H., Bange, H. W., et al. (2015). N-loss isotope effects in the Peru oxygen minimum zone studied using a mesoscale eddy as a natural tracer experiment: N-LOSS ISOTOPE EFFECTS IN AN EDDY. *Global Biogeochemical Cycles* 29 (6), 793–811. doi: 10.1002/2014GB005001

Braman, R. S., and Hendrix, S. A. (1989). Nanogram nitrite and nitrate determination in environmental and biological materials by vanadium(III) reduction with chemiluminescence detection. *Analytical Chem.* 61 (24), 2715–2718. doi: 10.1021/ac00199a007

Brandes, J. A., and Devol, A. H. (2002). A global marine-fixed nitrogen isotopic budget: Implications for Holocene nitrogen cycling: NITROGEN ISOTOPIC BUDGET. *Global Biogeochemical Cycles* 16 (4), 67-1-67–14. doi: 10.1029/2001GB001856

Buesseler, K. O., Antia, A. N., Chen, M., Fowler, S. W., Gardner, W. D., Gustafsson, O., et al. (2007). An assessment of the use of sediment traps for estimating upper ocean particle fluxes. *J. Mar. Res.* 65 (3), 345–416. doi: 10.1357/002224007781567621

Caffin, M., Moutin, T., Foster, R.A., Bouruet-Aubertot, P., Doglioli, A.M., Berthelot, H., et al. (2018). N_2 fixation as a dominant new N source in the western tropical South Pacific Ocean (OUTPACE cruise). *Biogeosciences* 15 (8), 2565–2585. doi: 10.5194/bg-15-2565-2018

Capone, D. G. (2001). Marine nitrogen fixation: what's the fuss? *Curr. Opin. Microbiol.* 4 (3), 341–348. doi: 10.1016/S1369-5274(00)00215-0

Capone, D. G., Zehr, J. P., Paerl, H. W., Bergman, B., and Carpenter, E. J. (1997). *Trichodesmium* , a globally significant marine cyanobacterium. *Science* 276 (5316), 1221–1229. doi: 10.1126/science.276.5316.1221

Capone, D. G., Burns, J. A., Montoya, J. P., Subramaniam, A., Mahaffey, C., Gunderson, T., et al. (2005). Nitrogen fixation by *Trichodesmium* spp.: An important source of new nitrogen to the tropical and subtropical North Atlantic Ocean: NITROGEN FIXATION IN THE NORTH ATLANTIC. *Global Biogeochemical Cycles* 19 (2). doi: 10.1029/2004GB002331

Capone, D. G., Ferrier, M. D., and Carpenter, E. J. (1994). Amino acid cycling in colonies of the planktonic marine cyanobacterium *trichodesmium thiebautii*. *Appl. Environ. Microbiol.* 60 (11), 3989–3995. doi: 10.1128/aem.60.11.3989-3995.1994

Carpenter, E. J., Harvey, H. R., Fry, B., and Capone, D. G. (1997). Biogeochemical tracers of the marine cyanobacterium Trichodesmium. *Deep Sea Res. Part I: Oceanographic Res. Papers* 44 (1), 27–38. doi: 10.1016/S0967-0637(96)00091-X

Casciotti, K. L., Buchwald, C., and McIlvin, M. (2013). Implications of nitrate and nitrite isotopic measurements for the mechanisms of nitrogen cycling in the Peru oxygen deficient zone. *Deep Sea Res. Part I: Oceanographic Res. Papers* 80, 78–93. doi: 10.1016/j.dsr.2013.05.017

Casciotti, K. L., Sigman, D. M., Böhlke, J.K., and Hilkert, A. (2002). Measurement of the oxygen isotopic composition of nitrate in seawater and freshwater using the denitrifier method. *Analytical Chem.* 74 (19), 4905–4912. doi: 10.1021/ac020113w

Casciotti, K. L., Trull, T. W., Glover, D. M., and Davies, D. (2008). Constraints on nitrogen cycling at the subtropical North Pacific Station ALOHA from isotopic measurements of nitrate and particulate nitrogen. *Deep Sea Res. Part II: Topical Stud. Oceanography* 55 (14–15), 1661–1672. doi: 10.1016/j.dsr2.2008.04.017

Confesor, K. A., Selden, C. R., Powell, K. E., Donahue, L. A., Mellett, T., Caprara, S., et al. (2022). Defining the realized niche of the two major clades of trichodesmium: A study on the west florida shelf. *Front. Mar. Sci.* 9, 821655. doi: 10.3389/fmars.2022.821655

Conway, T. M., and John, S. G. (2014). Quantification of dissolved iron sources to the North Atlantic Ocean. *Nature* 511 (7508), 212–215. doi: 10.1038/nature13482

Dekaezemacker, J., Bonnet, S., Grosso, O., Moutin, T., Bressac, M., and Capone, D. G. (2013). Evidence of active dinitrogen fixation in surface waters of the eastern tropical South Pacific during El Niño and La Niña events and evaluation of its potential nutrient controls: N $_2$ FIXATION IN THE ETSP. *Global Biogeochemical Cycles* 27 (3), 768–779. doi: 10.1002/gbc.20063

Deutsch, C., Sigman, D. M., Thunell, R. C., Meckler, A. N., and Haug, G. H. (2004). Isotopic constraints on glacial/interglacial changes in the oceanic nitrogen budget: GLACIAL/INTERGLACIAL NITROGEN BUDGET. *Global Biogeochemical Cycles* 18 (4). doi: 10.1029/2003GB002189

de Verneil, A., Rousselet, L., Doglioli, A. M., Petrenko, A. A., and Moutin, T. (2017). The fate of a southwest Pacific bloom: gauging the impact of submesoscale vs. mesoscale circulation on biological gradients in the subtropics. *Biogeosciences* 14 (14), 3471–3486. doi: 10.5194/bg-14-3471-2017

Dore, J. E., Brum, J. R., Tupas, L. M., and Karl, D. M. (2002). Seasonal and interannual variability in sources of nitrogen supporting export in the oligotrophic subtropical North Pacific Ocean. *Limnology Oceanography* 47 (6), 1595–1607. doi: 10.4319/lo.2002.47.6.1595

Dugdale, R. C., and Goering, J. J. (1967). Uptake of new and regenerated forms of nitrogen in primary productivity1: uptake of nitrogen in primary productivity. *Limnology Oceanography* 12 (2), 196–206. doi: 10.4319/lo.1967.12.2.0196

Dutkiewicz, S., Ward, B. A., Monteiro, F., and Follows, M. J. (2012). Interconnection of nitrogen fixers and iron in the Pacific Ocean: Theory and numerical simulations: MARINE NITROGEN FIXERS AND IRON. *Global Biogeochemical Cycles* 26 (1). doi: 10.1029/2011GB004039

Glibert, P. M., and Bronk, D. A. (1994). Release of dissolved organic nitrogen by marine diazotrophic cyanobacteria, trichodesmium spp.t. *Appl. Environ. Microbiol.* 60, 3996–4000. doi: 10.1128/aem.60.11.3996-4000.1994

Gruber, N. (2004). "The dynamics of the marine nitrogen cycle and its influence on atmospheric CO2 variations," in *The ocean carbon cycle and climate*. Eds. M. Follows and T. Oguz (Dordrecht: Springer Netherlands), 97–148. doi: 10.1007/978-1-4020-2087-2_4

Guieu, C., Bonnet, S., Petrenko, A., Menkes, C., Chavagnac, V., Desboeufs, K., et al. (2018). Iron from a submarine source impacts the productive layer of the Western Tropical South Pacific (WTSP). *Sci. Rep.* 8 (1), 9075. doi: 10.1038/s41598-018-27407-z

Hoering, T. C., and Ford, H. T. (1960). The isotope effect in the fixation of nitrogen by azotobacter. *J. Am. Chem. Soc.* 82 (2), 376–378. doi: 10.1021/ja01487a031

Jickells, T. D., An, Z. S., Andersen, K. K., Baker, A. R., Bergametti, G., Brooks, N., et al. (2005). Global iron connections between desert dust, ocean biogeochemistry, and climate. *Science* 308 (5718), 67–71. doi: 10.1126/science.1105959

Karl, D., Letelier, R., Tupas, L., Dore, J., Christian, J., and Hebel, D. (1997). The role of nitrogen fixation in biogeochemical cycling in the subtropical North Pacific Ocean. *Nature* 388 (6642), 533–538. doi: 10.1038/41474

Knapp, A. N., DiFiore, P. J., Deutsch, C., Sigman, D. M., and Lipschultz, F. (2008). Nitrate isotopic composition between Bermuda and Puerto Rico: Implications for N $_2$ fixation in the Atlantic Ocean: SARGASSO SEA NITRATE ISOTOPES. *Global Biogeochemical Cycles* 22 (3). doi: 10.1029/2007GB003107

Knapp, A. N., Casciotti, K. L., Berelson, W. M., Prokopenko, M. G., and Capone, D. G. (2016a). Low rates of nitrogen fixation in eastern tropical South Pacific surface waters. *Proc. Natl. Acad. Sci.* 113 (16), 4398–4403. doi: 10.1073/pnas.1515641113

Knapp, A. N., Fawcett, S.E., Martínez-Garcia, A., Leblond, N., Moutin, T., and Bonnet, S. (2016b). Nitrogen isotopic evidence for a shift from nitrate- to diazotroph-fueled export production in the VAHINE mesocosm experiments. *Biogeosciences* 13 (16), 4645–4657. doi: 10.5194/bg-13-4645-2016

Knapp, A. N., McCabe, K.M., Grosso, O., Leblond, N., Moutin, T., and Bonnet, S. (2018). Distribution and rates of nitrogen fixation in the western tropical South Pacific Ocean constrained by nitrogen isotope budgets. *Biogeosciences* 15 (9), 2619–2628. doi: 10.5194/bg-15-2619-2018

Knapp, A. N., Thomas, R. K., Stukel, M.R., Kelly, T.B., Landry, M.R., Selph, K.E., et al. (2021). Constraining the sources of nitrogen fueling export production in the Gulf of Mexico using nitrogen isotope budgets. *J. Plankton Res.* 44 (5), 692–710. doi: 10.1093/plankt/fbab049

Knapp, A. N., and Forrer, H. J. (2023). Water column nitrate plus nitrite d15N measurements from seawater collected in November 2019 and November 2020 in the Western Tropical South Pacific. *Biol. Chem. Oceanography Data Manage. Office (BCO-DMO)*. doi: 10.26008/1912/bco-dmo.869963.2

Kruskal, W. H., and Wallis, W. A. (1952). Use of ranks in one-criterion variance analysis. *J. Am. Stat. Assoc.* 47, 583–621. 40. doi: 10.1080/01621459.1952.10483441

Kustka, A., Saudo-Wilhelmy, S., Carpenter, E. J., Capone, D. G., and Raven, J. A. (2003). A revised estimate of the iron use efficiency of nitrogen fixation, with special reference to the marine cyanobacterium *trichodesmium* spp. (cyanophyta) [1]. *J. Phycology* 39 (1), 12–25. doi: 10.1046/j.1529-8817.2003.01156.x

Landolfi, A., Kähler, P., Koeve, W., and Oschlies, A. (2018). Global marine N2 fixation estimates: from observations to models. *Front. Microbiol.* 9, 2112. doi: 10.3389/fmicb.2018.02112

Lehmann, N., Granger, J., Kienast, M., Brown, K. S., Rafter, P. A., Martínez-Méndez, G., et al. (2018). Isotopic evidence for the evolution of subsurface nitrate in the western equatorial pacific. *J. Geophysical Research: Oceans* 123 (3), 1684–1707. doi: 10.1002/2017JC013527

Lory, C., Guieu, C., Rodier, M., Planquette, H., Gonzales Santana, D., Sarthou, G., et al. Environmental drivers of diazotrophs biogeography in the subtropical South Pacific Ocean. *Front Mar Sci* (2023). Available at: https://campagnes.flotteoceanographique.fr/campagnes/18000884/.

Luo, Y.-W., Doney, S. C., Anderson, L. A., Benavides, M., Berman-Frank, I., Bode, A., et al. (2012). Database of diazotrophs in global ocean: abundance, biomass and nitrogen fixation rates. *Earth System Sci. Data* 4 (1), 47–73. doi: 10.5194/essd-4-47-2012

Mahaffey, C. (2005). The conundrum of marine N2 fixation. *Am. J. Sci.* 305 (6–8), 546–595. doi: 10.2475/ajs.305.6-8.546

Mahowald, N. M., Baker, A. R., Bergametti, G., Brooks, N., Duce, R. A., Jickells, T. D., et al. (2005). Atmospheric global dust cycle and iron inputs to the ocean: ATMOSPHERIC IRON DEPOSITION. *Global Biogeochemical Cycles* 19 (4). doi: 10.1029/2004GB002402

Marconi, D., Sigman, D. M., Casciotti, K. L., Campbell, E. C., Alexandra Weigand, M., et al. (2017). Tropical dominance of N $_2$ fixation in the north atlantic ocean: tropical lead of atlantic N $_2$ fixation. *Global Biogeochemical Cycles* 31 (10), 1608–1623. doi: 10.1002/2016GB005613

Martin, J. H., Knauer, G. A., Karl, D. M., and Broenkow, W. W. (1987). VERTEX: carbon cycling in the northeast Pacific. *Deep Sea Res. Part A. Oceanographic Res. Papers* 34 (2), 267–285. doi: 10.1016/0198-0149(87)90086-0

McIlvin, M. R., and Casciotti, K. L. (2011). Technical updates to the bacterial method for nitrate isotopic analyses. *Analytical Chem.* 83 (5), 1850–1856. doi: 10.1021/ac1028984

Meiler, S., Britten, G. L., Dutkiewicz, S., Gradoville, M. R., Moisander, P. H., Jahn, O., et al. (2022). Constraining uncertainties of diazotroph biogeography from *nifH* gene abundance. *Limnology Oceanography* 67 (4), 816–829. doi: 10.1002/lno.12036

Minagawa, M., and Wada, E. (1986). Nitrogen isotope ratios of red tide organisms in the East China Sea: A characterization of biological nitrogen fixation. *Marine Chem.* 19 (3), 245–259. doi: 10.1016/0304-4203(86)90026-5

Moisander, P. H., Beinart, R.A., Hewson, I., White, A. E., Johnson, K. S., Carlson, C. A., et al. (2010). Unicellular cyanobacterial distributions broaden the oceanic N $_2$ fixation domain. *Science* 327 (5972), 1512–1514. doi: 10.1126/science.1185468

Moisander, P. H., Serros, T., Paerl, R. W., Beinart, R. A., and Zehr, J. P. (2014). Gammaproteobacterial diazotrophs and nifH gene expression in surface waters of the South Pacific Ocean. *ISME J.* 8 (10), 1962–1973. doi: 10.1038/ismej.2014.49

Monteiro, F. M., Dutkiewicz, S., and Follows, M. J. (2011). Biogeographical controls on the marine nitrogen fixers: CONTROLS ON MARINE NITROGEN FIXERS. *Global Biogeochemical Cycles* 25 (2). doi: 10.1029/2010GB003902

Montoya, J. P., Holl, C. M., Zehr, J. P., Hansen, A., Villareal, T. A., and Capone, D. G. (2004). High rates of N2 fixation by unicellular diazotrophs in the oligotrophic Pacific Ocean. *Nature* 430 (7003), 1027–1031. doi: 10.1038/nature02824

Moore Mills, M. M., Achterberg, E. P., Geider, R. J., LaRoche, J., Lucas, M. I., McDonagh, E. L., et al. (2009). Large-scale distribution of Atlantic nitrogen fixation controlled by iron availability. *Nat. Geosci.* 2 (12), 867–871. doi: 10.1038/ngeo667

Moutin, T., Wagener, T., Caffin, M., Fumenia, A., Gimenez, A., Baklouti, M., et al. (2018). Nutrient availability and the ultimate control of the biological carbon pump in the western tropical South Pacific Ocean. *Biogeosciences* 15, 2961–2989. doi: 10.5194/bg-2017-565

Mulholland, B., and Capone, D. (2004). Dinitrogen fixation and release of ammonium and dissolved organic nitrogen by Trichodesmium IMS101. *Aquat. Microbial Ecol.* 37, 85–94. doi: 10.3354/ame037085

Mulholland, M. R., Bernhardt, P. W., Widner, B. N., Selden, C. R., Chappell, P. D., Clayton, S., et al. (2019). High rates of N $_2$ fixation in temperate, western north atlantic coastal waters expand the realm of marine diazotrophy. *Global Biogeochemical Cycles* 33 (7), 826–840. doi: 10.1029/2018GB006130

Peters, B., Horak, R., Devol, A., Fuchsman, C., Forbes, M., Mordy, C. W., et al. (2018). Estimating fixed nitrogen loss and associated isotope effects using concentration and isotope measurements of NO3–, NO2–, and N2 from the Eastern Tropical South Pacific oxygen deficient zone. *Deep Sea Res. Part II: Topical Stud. Oceanography* 156, 121–136. doi: 10.1016/j.dsr2.2018.02.011

Raes, E. J., van de Kamp, J., Bodrossy, L., Fong, A. A., Riekenberg, J., Holmes, B. H., et al. (2020). N2 fixation and new insights into nitrification from the ice-edge to the equator in the south pacific ocean. *Front. Mar. Sci.* 7, 389. doi: 10.3389/fmars.2020.00389

Shao, Z., Xu, Y., Wang, H., Luo, W., Wang, L., Huang, Y., et al. (2023). Global oceanic diazotroph database version 2 and elevated estimate of global oceanic N2 fixation. *Earth System Science Data* 15 (8), 3673–3709. doi: 10.5194/essd-15-3673-2023

Siegel, D. A., and Deuser, W. G. (1997). Trajectories of sinking particles in the Sargasso Sea: modeling of statistical funnels above deep-ocean sediment traps. *Deep Sea Res. Part I: Oceanographic Res. Papers* 44 (9–10), 1519–1541. doi: 10.1016/S0967-0637(97)00028-9

Siegel, D. A., Fields, E., and Buesseler, K. O. (2008). A bottom-up view of the biological pump: Modeling source funnels above ocean sediment traps. *Deep Sea Res. Part I: Oceanographic Res. Papers* 55 (1), 108–127. doi: 10.1016/j.dsr.2007.10.006

Sigman, D. M., Casciotti, K. L., Andreani, M., Barford, C., Galanter, M., and Böhlke, J. K. (2001). A bacterial method for the nitrogen isotopic analysis of nitrate in seawater and freshwater. *Anal. Chem.* 73 (17), 4145–4153. doi: 10.1021/ac010088e

Smith, J. M., Chavez, F. P., and Francis, C. A. (2014). Ammonium uptake by phytoplankton regulates nitrification in the sunlit ocean. *PloS One* 9 (9), e108173. doi: 10.1371/journal.pone.0108173

Sohm, J. A., Webb, E. A., and Capone, D. G. (2011). Emerging patterns of marine nitrogen fixation. *Nat. Rev. Microbiol.* 9 (7), 499–508. doi: 10.1038/nrmicro2594

Staal, M., Meysman, F. J. R., and Stal, L. J. (2003). Temperature excludes N2-fixing heterocystous cyanobacteria in the tropical oceans. *Nature* 425 (6957), 504–507. doi: 10.1038/nature01999

Stenegren, M., Caputo, A., Berg, C., Bonnet, S., and Foster, R. A. (2018). Distribution and drivers of symbiotic and free-living diazotrophic cyanobacteria in the western tropical South Pacific. *Biogeosciences* 15 (5), 1559–1578. doi: 10.5194/bg-15-1559-2018

Talley, L. D., Pickard, G. L., Emery, W. J., and Swift, J. H. (2011). *Descriptive physical oceanography: an introduction. 6th ed* (Amsterdam ; Boston: Academic Press).

Tilliette, C., Gazeau, F., Chavagnac, V., Leblond, N., Montanes, M., Leblanc, K., et al. (2023). Temporal and spatial variability in the hydrothermal signature of sinking particles and sediments in the Western Tropical South Pacific Ocean. *ESS Open Archive*. doi: 10.22541/essoar.167898492.26733124/v1

Tilliette, C., Taillandier, V., BouruetAubertot, P., Grima, N., Maes, C., Montanes, M., et al. (2022). Dissolved iron patterns impacted by shallow hydrothermal sources along a transect through the Tonga-kermadec arc. *Global Biogeochemical Cycles* 36, e2022GB007363. doi: 10.1029/2022GB007363

Turk-Kubo, K. A., Achilles, K. M., Serros, T. R. C., Ochiai, M., Montoya, J. P., Zehr, J. P., et al. (2012). Nitrogenase (nifH) gene expression in diazotrophic cyanobacteria in the Tropical North Atlantic in response to nutrient amendments. *Front. Microbiol.* 3. doi: 10.3389/fmicb.2012.00386

Waniek, J., Koeve, W., and Prien, R. D. (2000). Trajectories of sinking particles and the catchment areas above sediment traps in the northeast Atlantic. *J. Mar. Res.* 58 (6), 983–1006. doi: 10.1357/002224000763485773

Webb, D. J. (2000). Evidence for shallow zonal jets in the south equatorial current region of the southwest pacific. *J. Phys. Oceanography* 30, 15. doi: 10.1175/1520-0485(2000)030<0706:EFSZJI>2.0.CO;2

Weber, T., and Deutsch, C. (2014). Local versus basin-scale limitation of marine nitrogen fixation. *Proc. Natl. Acad. Sci.* 111 (24), 8741–8746. doi: 10.1073/pnas.1317193111

Weigand, M. A., Foriel, J., Barnett, B., Oleynik, S., and Sigman, D. M. (2016). Updates to instrumentation and protocols for isotopic analysis of nitrate by the denitrifier method. *Rapid Commun. Mass Spectrometry* 30 (12), 1365–1383. doi: 10.1002/rcm.7570

White, A. E., Foster, R. A., Benitez-Nelson, C. R., Masqué, P., Verdeny, E., Popp, B. N., et al. (2013). Nitrogen fixation in the gulf of california and the eastern tropical north pacific. *Prog. Oceanography* 109, 1–17. doi: 10.1016/j.pocean.2012.09.002

White, A. E., Granger, J., Selden, C., Gradoville, M.R., Potts, L., Bourbonnais, A., et al. (2020). A critical review of the $^{15}N_2$ tracer method to measure diazotrophic production in pelagic ecosystems. *Limnology Oceanography: Methods* 18 (4), 129–147. doi: 10.1002/lom3.10353

Xu, H., and Weber, T. (2021). Ocean dust deposition rates constrained in a data-assimilation model of the marine aluminum cycle. *Global Biogeochemical Cycles* 35 (9). doi: 10.1029/2021GB007049

Zehr, J. P., Mellon, M. T., and Zani, S. (1998). New nitrogen-fixing microorganisms detected in oligotrophic oceans by amplification of nitrogenase (nifH) genes. *Appl. Environ. Microbiol.* 64 (9), 3444–3450. doi: 10.1128/AEM.64.9.3444-3450.1998

Zehr, J. P., and Turner, (2001) *Nitrogen fixation: Nitrogenase genes and gene expression - ScienceDirect*. Available at: https://www.sciencedirect.com/science/article/abs/pii/S0580951701300491?via%3Dihub (Accessed 14 February 2023).